The association for medical ultrasound
aium
AMERICAN INSTITUTE OF ULTRASOUND IN MEDICINE

CME Course
POWERED BY THE AIUM

AMERICAN INSTITUTE OF ULTRASOUND IN MEDICINE (AIUM)

Advanced OB-GYN Ultrasound Seminar

February 20–23, 2019 | Disney's Yacht and Beach Club Resorts | Lake Buena Vista, FL

Register to attend in-person or live stream

REGISTER TODAY!

American Institute of Ultrasound in Medicine
14750 Sweitzer Ln , Suite 100
Laurel, MD 20707
aium.org | 800-638-5352

IN PARTNERSHIP WITH

ORLANDO HEALTH

Wake Forest® School of Medicine

Repeatability and Reproducibility of the Ultrasonic Attenuation Coefficient and Backscatter Coefficient Measured in the Right Lobe of the Liver in Adults With Known or Suspected Nonalcoholic Fatty Liver Disease

Aiguo Han, PhD, Michael P. Andre, PhD, Lisa Deiranieh, BS, RDMS, Elise Housman, BS, RDMS, John W. Erdman, Jr PhD, Rohit Loomba, MD, MHSc, Claude B. Sirlin, MD, William D. O'Brien, Jr, PhD

Received May 23, 2017, from the Bioacoustics Research Laboratory, Department of Electrical and Computer Engineering (A.H., W.D.O.), and Department of Food Science and Human Nutrition (J.W.E.), University of Illinois at Urbana-Champaign, Urbana, Illinois USA; Department of Radiology, University of California, San Diego, and San Diego VA Healthcare System, San Diego, California USA (M.P.A., L.D., E.H.); and Nonalcoholic Fatty Liver Disease Research Center, Division of Gastroenterology (R.L.), and Department of Radiology (C.B.S.), University of California, San Diego, La Jolla, California USA. Manuscript accepted for publication October 22, 2017.

This work was supported in part by National Institutes of Health/National Institute of Diabetes and Digestive and Kidney Diseases grant 5R01DK106419 and a grant from Siemens Medical Solutions, Inc.

Address correspondence to William D. O'Brien, Jr, PhD, Bioacoustics Research Laboratory, Department of Electrical and Computer Engineering, University of Illinois at Urbana-Champaign, 306 N Wright St, Urbana, IL 61801 USA.

E-mail: wdo@uiuc.edu

Abbreviations

AC, attenuation coefficient; BMI, body mass index; BSC, backscatter coefficient; CI, confidence interval; CV, coefficient of variation; FOI, field of interest; ICC, intraclass correlation coefficient; NAFLD, nonalcoholic fatty liver disease; PDFF, proton density fat fraction; QIBA, Quantitative Imaging Biomarker Alliance; QUS, quantitative ultrasound; RC, repeatability coefficient; RDC, reproducibility coefficient; RF, radiofrequency; ROI, region of interest; R&R, repeatability and reproducibility; SD, standard deviation

doi:10.1002/jum.14537

Objectives—To assess the repeatability and reproducibility of the ultrasonic attenuation coefficient (AC) and backscatter coefficient (BSC) measured in the livers of adults with known or suspected nonalcoholic fatty liver disease (NAFLD).

Methods—The Institutional Review Board approved this Health Insurance Portability and Accountability Act–compliant prospective study; informed consent was obtained. Forty-one research participants with known or suspected NAFLD were recruited and underwent same-day ultrasound examinations of the right liver lobe with a clinical scanner by a clinical sonographer. Each participant underwent 2 scanning trials, with participant repositioning between trials. Two transducers were used in each trial. For each transducer, machine settings were optimized by the sonographer but then kept constant while 3 data acquisitions were obtained from the liver without participant repositioning and then from an external calibrated phantom. Raw RF echo data were recorded. The AC and BSC were measured within 2.6 to 3.0 MHz from a user-defined hepatic field of interest from each acquisition. The repeatability and reproducibility were analyzed by random-effects models.

Results—The mean AC and log-transformed BSC (logBSC) were 0.94 dB/cm-MHz and –27.0 dB, respectively. Intraclass correlation coefficients were 0.88 to 0.94 for the AC and 0.87 to 0.95 for the logBSC acquired without participant repositioning. For between-trial repeated scans with participant repositioning, the intraclass correlation coefficients were 0.80 to 0.84 for the AC and 0.69 to 0.82 for the logBSC after averaging results from 3 within-trial images. The variability introduced by the transducer was less than the repeatability error.

Conclusions—Hepatic AC and BSC measures using a reference phantom technique on a clinical scanner are repeatable and reproducible between transducers in adults with known or suspected NAFLD.

Key Words—fatty liver disease; gastrointestinal; repeatability; reproducibility; ultrasonic attenuation coefficient; ultrasonic backscatter coefficient; ultrasound techniques/physics

Under technical development for decades, quantitative ultrasound (QUS) now is emerging as a noninvasive means to objectively assess human diseases and conditions, with

promising potential applications: for example, in liver fat quantification,[1–3] spontaneous preterm birth prediction,[4,5] and breast cancer treatment monitoring.[6] The US attenuation coefficient (AC, dB/cm-MHz) and US backscatter coefficient (BSC, $[\text{cm-sr}]^{-1}$) are two fundamental QUS parameters derived from the raw radiofrequency (RF) echo data. The AC is a measure of US energy loss in tissue and provides a numerical parameter analogous to the obscuration of tissue structures assessed qualitatively from B-mode images. The BSC is a measure of US energy returned from tissue and provides a quantitative parameter analogous to the "echogenicity" assessed qualitatively from B-mode images. The two parameters promise to be clinically useful quantitative imaging biomarkers, a term defined by the Radiological Society of North America's Quantitative Imaging Biomarker Alliance (QIBA) as "a characteristic derived from one or more in vivo images and objectively measured according to a ratio or interval scale as an indicator of normal biological processes, pathogenic processes, or response to a therapeutic intervention."[7]

Nonalcoholic fatty liver disease (NAFLD) is one of the most common types of chronic liver diseases worldwide.[8] Noninvasive assessment of disease severity in NAFLD is an area of intense research.[9] The magnetic resonance imaging (MRI)-measured proton density fat fraction (PDFF) is emerging as an accurate and reproducible quantitative biomarker for assessment and quantification of liver fat content in patients with NAFLD,[9–13] but MRI is not widely available globally, and it can provoke anxiety or be unsafe in some patients. The controlled attenuation parameter measured by FibroScan (Echosens, Paris, France) has promise for objective assessment of liver fat in NAFLD, but this method has several limitations, including low accuracy to distinguish between different grades of hepatic steatosis.[14,15] Also, the controlled attenuation parameter is a proprietary algorithm provided by a single manufacturer used on a specialized device, and it is not available on most clinical US systems. Current conventional US image-based assessment of liver fat is not accurate and lacks objectivity and precision because of system and reader variability. Recent studies using the AC and BSC have shown promise in fat quantification.[1–3]

For the AC and BSC to play important roles as clinically useful quantitative imaging biomarkers, both technical and clinical performance of the parameters need to be evaluated rigorously. Repeatability and reproducibility (R&R) are two technical performance metrics that address quantitative imaging biomarker precision. Repeatability is "the measurement of precision with conditions that remain unchanged between replicate measurements (repeatability conditions),"[7] whereas reproducibility is "the measurement of precision with conditions that vary between replicate measurements (reproducibility conditions)."[7] The measurement location in the liver, operator, and measurement systems are examples of reproducibility conditions. A previous study showed good repeatability and operator/transducer reproducibility of the AC and BSC in homogeneous liver-mimicking phantoms.[16] Furthermore, previous work showed that the AC and BSC may accurately diagnose hepatic steatosis in adults with known or suspected NAFLD.[1] However, R&R of the AC and BSC in in vivo human NAFLD have not been examined. Therefore, this study's purpose was to assess R&R of the AC and BSC in adults with known or suspected NAFLD.

Materials and Methods

Study Design and Participants

Institutional Review Board approval was obtained for this Health Insurance Portability and Accountability Act–compliant study. Forty-one adult research participants with known or suspected NAFLD were prospectively recruited between September 2015 and November 2016 from the University of California, San Diego's NAFLD Research Center. Other than known or suspected NAFLD, the only inclusion criterion was willingness to participate. Written informed consent was obtained. Demographic and anthropometric data were acquired by research coordinators. Data from contemporaneous hepatic MRI research studies and/or from clinical-care liver biopsies were recorded if available to help characterize the participant cohort.

Ultrasonic Data Acquisition

A clinical US system (S3000; Siemens Medical Solutions, Inc, Issaquah, WA) was used, which allowed recording of direct post–beam-formed RF echo data acquisition under terms of a research agreement. Two experienced registered diagnostic medical sonographers (A and B) performed a research protocol for liver assessment on 41 participants: 20 scanned by A, termed group A; and 21 scanned by B, termed group B.

Each participant underwent 2 repeated scanning trials (Figure 1), separated by 5 to 10 minutes, between

which the participant left the table and then was repositioned on the scanning table (referred to as participant repositioning). Each trial comprised 2 data acquisition sequences, 1 using a 4C1 transducer (1–4 MHz nominal) and the other a 6C1HD transducer (1.5-6 MHz nominal). Each sequence comprised 4 data acquisitions: 3 in the right liver lobe using a lateral intercostal approach and 1 in calibrated reference phantom P2 (details available in the "Reference Phantom" subsection). A data acquisition means a single-operator button press that recorded a B-mode image and RF data. Twelve liver images were collected per participant (Figure 1): 2 repeated trials × 2 transducers per trial × 3 repeated acquisitions per transducer.

In keeping with standard clinical practice, the sonographer adjusted system settings in each participant for a given transducer to optimize right hepatic lobe visualization and then acquired B-mode/RF data for that trial. Participants suspended breathing after shallow inspiration before each data acquisition. Since each acquisition was obtained during a separate breath hold about 15 seconds apart, minor repositioning of the transducer was unavoidable, although the sonographer attempted to replicate the same liver location.

Definitions of AC and BSC

Attenuation refers to the loss of wave amplitude due to all mechanisms (eg, absorption and scattering). For US wave propagation in human soft tissues, the amplitude decay may be modeled as $A(z)=A_0-\alpha fz$, where A_0 is the initial US wave amplitude (in dB); $A(z)$ is the amplitude (in dB) after the wave propagates a distance z (in cm); f is the US frequency (in MHz); and α is the AC (in dB/cm-MHz). αfz represents the total loss of wave amplitude.

The BSC is a measure of the ability of tissue to scatter US waves and provides a quantitative parameter analogous to the echogenicity assessed qualitatively from B-mode images. The BSC is defined as the differential scattering cross section per unit volume for a scattering angle of 180° (ie, backscattering direction). The logarithmically transformed version of the BSC is denoted in

Figure 1. Diagram of the design for data acquisition and processing. The machine settings remained constant within each data acquisition sequence (eg, the same machine settings were used for acquiring liver images a1, a2, and a3 and phantom image a) but were allowed to be changed from one acquisition sequence to the next or between participants.

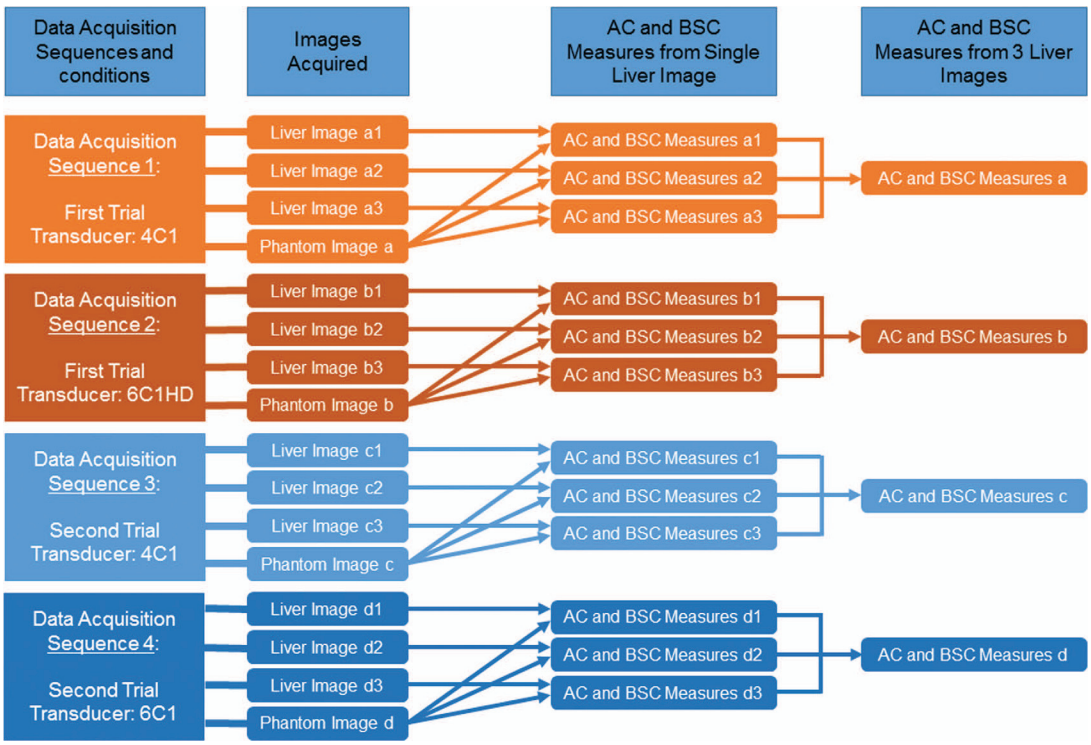

this article as logBSC (in dB), where $logBSC = 10log_{10}(BSC/BSC_0)$, with $BSC_0 = 1\ (\text{cm-sr})^{-1}$.

Reference Phantom

The reference phantom P2 was purchased from CIRS, Inc (Norfolk, VA). The model/project number of the phantom was 1409-00. The phantom was housed in a plastic cylinder with an inside dimension of 15 ± 1 cm and a height of 20 ± 0.5 cm. The bottom was potted in an acoustically absorbing polymer, 2 cm thick, whereas the top had a polyethylene laminate membrane approximately 200 μm thick. The top also had a water well extending approximately 2 cm above the membrane surface.

The calibrated speed of sound for phantom P2 was 1540 m/s between 2 and 4 MHz. The calibrated AC for phantom P2 was 0.69 dB/cm-MHz between 2 and 4 MHz. The calibrated BSC was frequency dependent. The BSC was $2.5 \times 10^{-4}\ (\text{cm-sr})^{-1}$ at 2.8 MHz (ie, logBSC = –36.0 dB), and the logBSC-versus-frequency plot between 2 and 4 MHz is shown in Figure 2. The QUS technique does not require multiple phantoms spanning the range of human liver AC and BSC values. Only a single phantom with a fixed AC and BSC is needed.

Attenuation Coefficient and BSC Computation

Attenuation coefficient and BSC frequency spectra were derived from the RF data of the liver and phantom by using established methods.[16,17] To do so, the liver and phantom RF data were transferred to a personal computer for offline processing (MATLAB; The MathWorks, Natick, MA). The liver B-mode image was reconstructed from the RF data. A field of interest (FOI) was drawn on each B-mode reconstruction, outlining the region inside the liver boundary (Figure 3) to gate the RF data. The FOI was required by the AC and BSC algorithms; the liver AC and BSC were computed by comparing the RF data of the liver with those of the calibrated phantom. The RF data outside the liver cannot be used, or the resultant AC and BSC would correspond to extrahepatic tissues rather than the liver. To keep the FOI drawing simple, which is likely to be relevant for possible future clinical applications of this technology, no effort was made to exclude any hepatic vessels. Fields of interest were drawn under the supervision of an expert radiologist by a physician fellow with 2 years of experience in radiologic body-imaging research and by a medical physicist with 4 decades of experience in US research.

The delineated FOI was analyzed to yield the AC and BSC estimates as described below. For both AC and BSC estimates, the FOI was subdivided into overlapping sub-regions of interest (ROIs). The AC sub-ROIs had a dimension of 20 mm × 40 A-lines (axial × lateral; axial size equivalent to 20 pulse lengths). The lateral and axial overlaps between adjacent AC sub-ROIs were both set to be 50%.[16] The BSC sub-ROIs had a dimension of 7.7 mm × 40 A-lines (axial × lateral; axial size equivalent to 15 wavelengths at 3 MHz). The lateral and axial overlaps between adjacent BSC sub-ROIs were both set to be 75%.[16] An AC spectrum was generated from each

Figure 2. LogBSC-versus-frequency plot for the reference phantom.

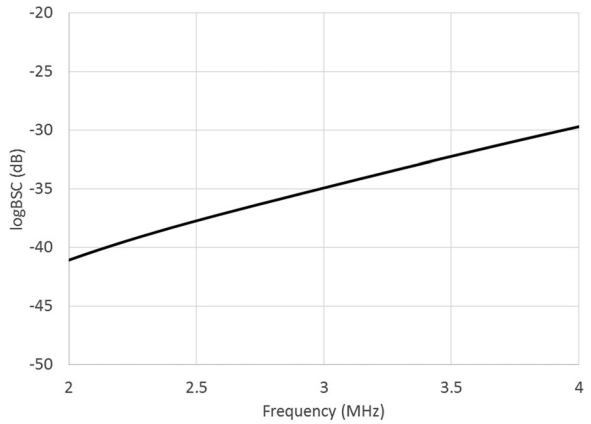

Figure 3. Representative liver B-mode image reconstructed from the RF data acquired from a 32-year-old man. The pink FOI line was drawn on the reconstructed B-mode image to delineate the liver boundary.

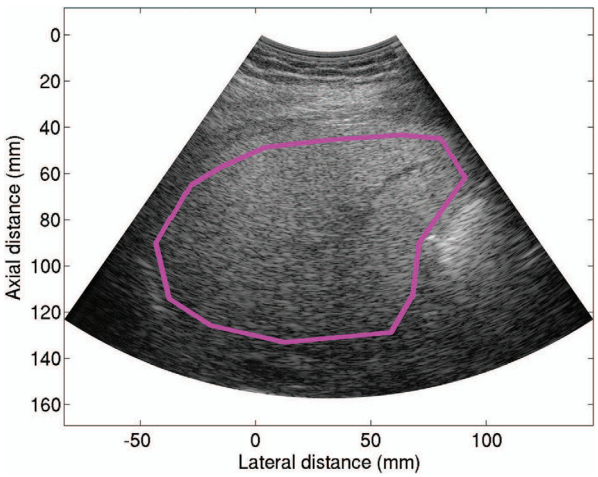

AC sub-ROI, and the results from all AC sub-ROIs within the FOI were averaged to yield the AC spectrum of the entire FOI. The BSC spectrum for the FOI was calculated likewise.

The spectral difference method was used to calculate the liver AC for an AC sub-ROI. Briefly, the AC sub-ROI was further divided into axial sections with a 50% axial overlap between adjacent axial sections, where each section represented a different depth. The liver power spectrum $S_{Liver}(f, z)$ was then estimated at each depth z by averaging the squared moduli of the fast Fourier transforms of all the A-lines in the subsection corresponding to that depth. The phantom power spectrum $S_{Phantom}(f, z)$ was also estimated for each depth for which the liver power spectrum was estimated, using a similar approach except that more A-lines were used for the phantom power spectrum estimate to reduce noise. More A-lines were a result of laterally extending the sub-ROIs and subsections for the phantom (not exceeding the phantom edge), taking advantage of the spatial uniformity of the phantom. Finally, the AC spectrum for an AC sub-ROI was estimated by

$$AC_{Liver}(f) = AC_{Phantom}(f) - \frac{\gamma(f)}{4 \times 8.686 f},$$

where $\gamma(f)$ is the slope of the straight line that fits the log spectrum difference $\log(S_{Liver}(f, z)) - \log(S_{Phantom}(f, z))$ as a function of depth, and the phantom AC, $AC_{Phantom}(f)$, was calibrated a priori.

The liver BSC was computed for each BSC sub-ROI without needing to further divide the BSC sub-ROI (a reason why the BSC sub-ROI was smaller than the AC sub-ROI). Instead, a single liver power spectrum estimate $S_{Liver}(f, z)$ was obtained for the BSC sub-ROI by averaging the squared moduli of the fast Fourier transforms of all the A-lines in the sub-ROI. The phantom power spectrum corresponding to the same depth, $S_{Phantom}(f, z)$, was obtained similarly from the phantom RF data, except that the phantom sub-ROI was extended laterally to reduce noise, similar to what was done for the AC estimate. The BSC spectrum for the BSC sub-ROI was then estimated using

$$BSC_{Liver}(f, z) = \frac{S_{Liver}(f, z)}{S_{Phantom}(f, z)} BSC_{Phantom}(f) 10^{2zf[AC_{Liver}(f) - AC_{Phantom}(f)]/10},$$

where $BSC_{Phantom}(f)$ was calibrated a priori, and the factor $10^{2zf[AC_{Liver}(f) - AC_{Phantom}(f)]/10}$ compensated for the attenuation effects.

Attenuation coefficient and BSC spectra were frequency averaged over a 2.6–3.0-MHz bandwidth, yielding single AC and BSC measures per image. The bandwidth was chosen because it was a narrow range around the 2.8-MHz center frequency of the transducers with an optimal signal-to-noise ratio. Averaging the measures from 3 images in an acquisition sequence yielded a 3-image measure. Both the single- and 3-image measures were analyzed.

Statistical Analysis

Statistical analysis was performed with R version 3.3.2 software (R Foundation for Statistical Computing, Vienna, Austria). Participant characteristics were summarized descriptively. The BSC was log transformed ($logBSC = 10log_{10}BSC$) for R&R assessment because logBSC was normally distributed. The AC and logBSC were assessed separately.

The between-image repeatability, between-trial repeatability, and between-transducer reproducibility were assessed for single-image measures. The between-trial repeatability and between-transducer reproducibility were assessed for 3-image measures. The repeatability was analyzed separately for various conditions because repeatability might depend on the conditions.

The repeatability was assessed by using a 1-way random-effects model[18]:

$$Y_{ij} = \mu + \mu_i + \varepsilon_{ij} (i = 1, \ldots, n_S; j = 1, \ldots, k), \qquad (1)$$

where there are n_S participants; Y_{ij} is the jth repeated measure from participant i; μ is the overall mean; and $\mu_i \sim N(0, \sigma_S^2)$ and $\varepsilon_{ij} \sim N(0, \sigma_E^2)$ are jointly independent random variables representing the random effects of the participants and replicates, respectively.

Table 1. Repeatability and Reproducibility Metrics and Their Representations Using Random-Effects Model Parameters

R&R Metrics	Between-Participant SD	Repeatability SD	RC	ICC(1,1)	QIBA Reproducibility SD	Gauge Reproducibility SD	RDC
Model representation	σ_S	σ_E	$2.77\sigma_E$	$\sigma_S^2/(\sigma_S^2+\sigma_E^2)$	$\sqrt{\sigma_T^2+\sigma_{ST}^2+\sigma_E^2}$	$\sqrt{\sigma_T^2+\sigma_{ST}^2}$	$2.77\sqrt{\sigma_T^2+\sigma_{ST}^2+\sigma_E^2}$

Following the Radiological Society of North America's QIBA suggestions, several repeatability metrics (Table 1) were calculated: repeatability standard deviation (SD) σ_E, coefficient of variation (CV) for AC, repeatability coefficient (RC = $2.77\sigma_E$),[19] and intraclass correlation coefficient (ICC) for absolute agreement. Two ICC forms were estimated: ICC(1,1) and ICC(1,k), representing values calculated from a single measure and from an average of k repeated measures, respectively.[20] In this study, $k = 3$.

The reproducibility was assessed by using a 2-way random-effects model[18]:

$$Y_{ijr} = \mu + \alpha_i + \beta_j + (\alpha\beta)_{ij} + \varepsilon_{ijr} (i = 1, \ldots, n_S; j = 1, \ldots, n_T; r = 1, \ldots, k), \quad (2)$$

where there are n_S participants and n_T transducers; Y_{ijr} is the rth repeated measure from participant i with transducer j; and $\alpha_i \sim N(0, \sigma_S^2)$, $\beta_i \sim N(0, \sigma_T^2)$, $(\alpha\beta)_{ij} \sim N(0, \sigma_{ST}^2)$, and $\varepsilon_{ijr} \sim N(0, \sigma_E^2)$ are jointly independent random variables representing the random effects of the participants, transducers, participant-by-transducer interactions, and replicates, respectively.

There are 2 widely used definitions of reproducibility. One includes the repeatability effect, whereas the other does not. Reproducibility that includes the repeatability effect is recommended by the QIBA and termed QIBA reproducibility herein. Reproducibility that excludes repeatability effect is popular in Gauge R&R studies and termed Gauge reproducibility[18] herein. The following reproducibility metrics were calculated: QIBA reproducibility SD ($\sqrt{\sigma_T^2 + \sigma_{ST}^2 + \sigma_E^2}$), reproducibility coefficient (RDC = $2.77\sqrt{\sigma_T^2 + \sigma_{ST}^2 + \sigma_E^2}$), and Gauge reproducibility SD ($\sqrt{\sigma_T^2 + \sigma_{ST}^2}$).

Results

Participants

Forty-one participants (26 female) were recruited from the University of California, San Diego's NAFLD Research Center, and those willing to participate were enrolled. The mean age was 55 (female, 59; male, 48) years, and the age range was 27 to 72 (female, 31–72; male, 27–68) years. The mean body mass index (BMI) was 30.1 kg/m^2, and the BMI range was 17.6 to 51.5 kg/m^2. The 20 group A participants included 7 men and 13 women with a mean BMI of 30.1 (range, 21.7–40.7) kg/m^2 and mean age of 56 (range, 31–72) years. The 21 group B participants included 8 men and 13 women with a mean BMI of 30.1 (range, 17.6–51.5) kg/m^2 and mean age of 53 (range, 27–71) years. Thirty-four of the 41 participants had MRI-PDFF measured within 0 to 277 (mean, 20) days of US; the mean MRI-PDFF was 14.3%, and the MRI-PDFF range was 3.2% to 40.0%. This MRI-PDFF range was comparable to a previous study with 204 participants.[1] Thirty-five participants had clinical-care liver biopsy within 1 to 283 (mean, 70) days of US with the following distribution of histologically determined steatosis grades: 2 participants with grade 0, 18 participants with grade 1, 12 participants with grade 2, and 3 participants with grade 3. The MRI-PDFF and histologically determined steatosis grade are presented to help characterize the participant cohort but were not included in subsequent analysis. The MRI-PDFF values show that the participant cohort covered a wide range of hepatic fat fractions. The histologically determined steatosis grades also show the broad steatosis spectrum of the study participants.

Attenuation Coefficient and BSC Measurement Results

Twelve single-image AC and 12 single-image logBSC measures were computed per participant. Box plots (Figure 4A and B) of all the single-image AC and logBSC measures were grouped by participant identification and ordered by BMI to provide an overview of the distribution and variability of the measures. Visual inspection of the box plots revealed that the within-participant variability was much smaller than the between-participant variability for both the AC and logBSC, indicating good overall R&R for the two parameters. Attenuation coefficient and logBSC values did not appear to be correlated with the BMI, nor was any correlation observed between the within-participant variability and the BMI. Therefore, the participant BMI did not seem to affect the AC and BSC outcomes.

The within-participant SDs for the single-image measures were plotted against the participant means in Figure 4C and D. No statistically significant linear correlation between the mean and SD was observed, suggesting that the absolute AC and logBSC levels would be unlikely to affect the R&R results. Therefore, the R&R results did not have to be reported at specified AC and logBSC levels.

Overall, the mean of the measured AC was 0.94 dB/cm-MHz, and that of the measured logBSC was –27.0 dB for the 41 participants. The average within-participant SD in the measured AC was 0.06 dB/cm-

MHz, and in the measured logBSC, it was 2.4 dB, with a CV of 6.9% for the AC; the CV was not applicable for the logBSC. The CV value for the AC was a small number that indicated good R&R. Notice that the CV is presented here for completeness. Although still useful, this measure was not as relevant when the SD was not correlated with the mean.

Between-Image Repeatability of Single-Image Measures

The between-image repeatability was assessed independently under various measurement conditions (ie, sonographer-transducer-trial combinations) by using the model described in Equation 1. For each condition, there were 20 or 21 participants and 3 replicate measures (3 images) per participant. The estimated between-participant SD, between-image repeatability SD, RC, ICC(1,1), and ICC(1,3) were summarized in Table 2 for each measurement condition. The estimates under different conditions were similar, with ICC(1,1) greater than 0.9 for most conditions and ICC(1,3) greater than 0.95 for all conditions. The ICCs of the AC were close to those of the logBSC.

Figure 4. Summary plots for the AC and logBSC results. The box plots show the single-image measures of AC (**A**) and logBSC (**B**) for all transducers, trials, and images, as ordered by participant BMI. The standard deviation versus the mean scatterplots show no linear correlation between the standard deviation and the mean of AC (**C**) and logBSC (**D**).

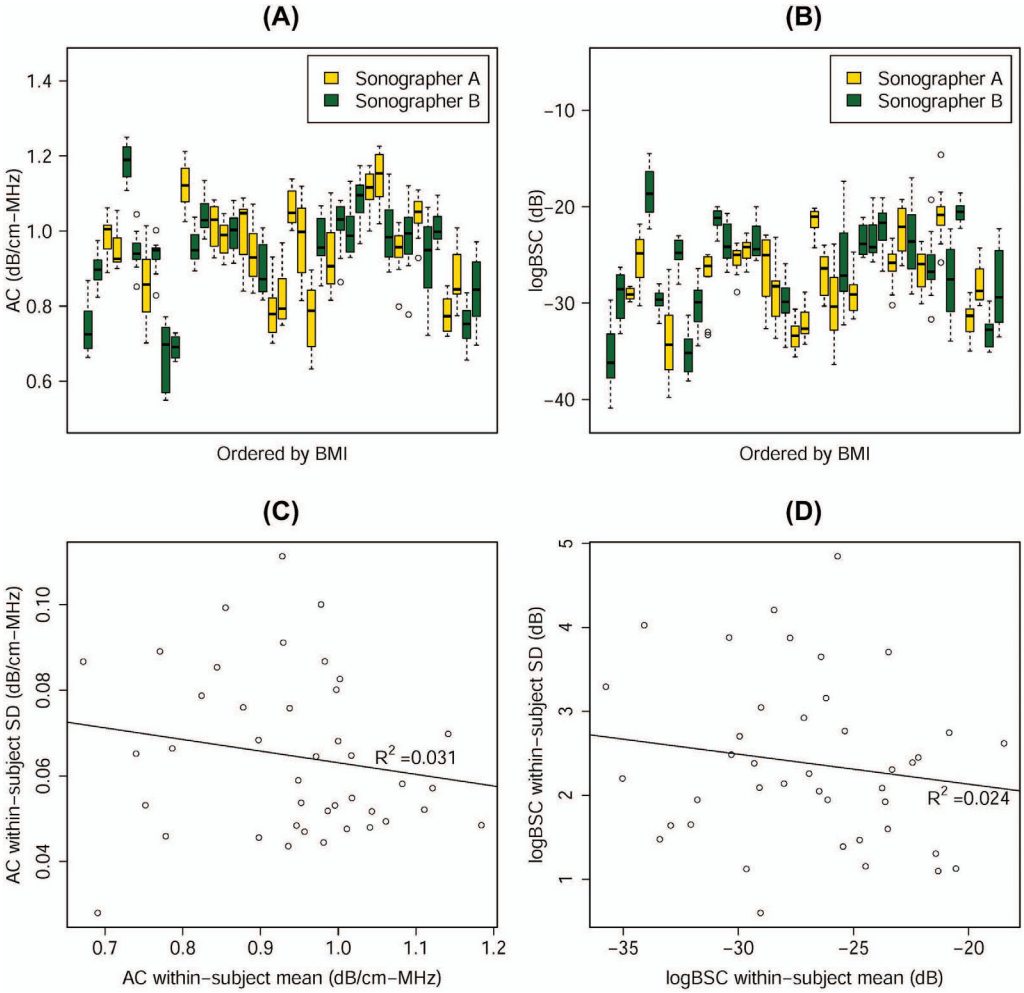

Table 2. Between-Image Repeatability Estimates for Single-Image AC and BSC Measures Obtained Under Various Conditions, Calculated by Using the 1-Way Random-Effects Model

Conditions			Summary Statistics for AC, dB/cm-MHz					ICC Estimates for AC	
Participant Group[a]	Transducer	Trial ID	Mean	Range	Between-Participant SD (95% CI)	Between-Image Repeatability SD (95% CI)	RC (95% CI)	ICC(1,1) (95% CI)[b]	ICC(1,3) (95% CI)[c]
A	4C1	1	0.94	0.69, 1.21	0.13 (0.10, 0.19)	0.04 (0.03, 0.05)	0.12 (0.10, 0.15)	0.91 (0.82, 0.96)	0.97 (0.93, 0.99)
A	4C1	2	0.94	0.63, 1.18	0.14 (0.10, 0.20)	0.03 (0.03, 0.04)	0.09 (0.08, 0.12)	0.94 (0.89, 0.98)	0.98 (0.96, 0.99)
A	6C1HD	1	0.97	0.75, 1.23	0.11 (0.08, 0.16)	0.03 (0.03, 0.04)	0.09 (0.07, 0.11)	0.92 (0.84, 0.96)	0.97 (0.94, 0.99)
A	6C1HD	2	0.96	0.72, 1.21	0.12 (0.09, 0.18)	0.04 (0.03, 0.05)	0.10 (0.09, 0.13)	0.92 (0.83, 0.96)	0.97 (0.94, 0.99)
B	4C1	1	0.93	0.69, 1.25	0.13 (0.10, 0.19)	0.04 (0.03, 0.05)	0.11 (0.09, 0.14)	0.91 (0.83, 0.96)	0.97 (0.93, 0.99)
B	4C1	2	0.93	0.66, 1.14	0.12 (0.09, 0.18)	0.04 (0.03, 0.05)	0.10 (0.08, 0.13)	0.92 (0.84, 0.96)	0.97 (0.94, 0.99)
B	6C1HD	1	0.93	0.58, 1.18	0.14 (0.11, 0.21)	0.05 (0.04, 0.07)	0.15 (0.12, 0.18)	0.88 (0.77, 0.94)	0.96 (0.91, 0.98)
B	6C1HD	2	0.93	0.55, 1.22	0.15 (0.12, 0.22)	0.05 (0.04, 0.06)	0.12 (0.10, 0.16)	0.92 (0.85, 0.96)	0.97 (0.94, 0.99)

Conditions			Summary Statistics for logBSC, dB					ICC Estimates for logBSC	
Participant Group[a]	Transducer	Trial ID	Mean	Range	Between-Participant SD (95% CI)	Between-Image Repeatability SD (95% CI)	RC (95% CI)	ICC(1,1) (95% CI)[b]	ICC(1,3) (95% CI)[c]
A	4C1	1	−28.18	−39.77, −20.17	4.40 (3.26, 6.51)	1.67 (1.37, 2.13)	4.62 (3.79, 5.91)	0.87 (0.76, 0.94)	0.95 (0.90, 0.98)
A	4C1	2	−28.16	−39.23, −20.32	4.40 (3.30, 6.47)	1.18 (0.97, 1.52)	3.28 (2.69, 4.20)	0.93 (0.87, 0.97)	0.98 (0.95, 0.99)
A	6C1HD	1	−27.29	−34.26, −19.67	3.55 (2.66, 5.23)	1.01 (0.83, 1.29)	2.78 (2.29, 3.56)	0.93 (0.85, 0.97)	0.97 (0.95, 0.99)
A	6C1HD	2	−26.38	−34.97, −14.63	4.20 (3.14, 6.19)	1.25 (1.02, 1.60)	3.45 (2.84, 4.42)	0.92 (0.84, 0.96)	0.97 (0.94, 0.99)
B	4C1	1	−27.26	−35.71, −16.82	4.53 (3.42, 6.58)	1.19 (0.98, 1.51)	3.28 (2.71, 4.17)	0.94 (0.87, 0.97)	0.98 (0.95, 0.99)
B	4C1	2	−27.44	−40.90, −19.07	5.23 (3.96, 7.60)	1.24 (1.02, 1.58)	3.44 (2.84, 4.37)	0.95 (0.89, 0.98)	0.98 (0.96, 0.99)
B	6C1HD	1	−25.73	−38.08, −17.00	5.18 (3.90, 7.54)	1.54 (1.27, 1.96)	4.27 (3.52, 5.43)	0.92 (0.84, 0.96)	0.97 (0.94, 0.99)
B	6C1HD	2	−25.48	−37.36, −14.49	5.48 (4.12, 7.98)	1.66 (1.37, 2.11)	4.61 (3.80, 5.86)	0.92 (0.84, 0.96)	0.97 (0.94, 0.99)

[a]Participant groups A and B represent participants scanned by sonographers A and B, respectively.
[b]ICC(1,1) and the 95% CI were calculated by using the "irr" package in R using the 1-way analysis of variance model, "agreement" type, and "single" unit.
[c]ICC(1,3) and the 95% CI were calculated by using the 1-way analysis of variance model, "agreement" type, and "average" unit.

The between-image repeatability represents very short-term repeatability; adjacent images were acquired around 15 seconds apart. The participant stayed on the scanning table and was not repositioned. This assessment is a more idealized repeatability test. The between-image repeatability SD was much lower than the between-participant SD. As a result, the ICC values were high, showing excellent short-term repeatability for both the AC and logBSC.

Theoretically, the repeatability measures could be different under different conditions. For example, transducer X might have better repeatability than transducer Y, etc. That factor was why the repeatability measures were analyzed separately for different conditions. The fact that ICC values were high for all conditions suggested that the short-term repeatability was excellent for all conditions examined. The similar ICC values between different conditions indicated that the short-term repeatability did not depend on which of the two transducers was used or on which of the two sonographers performed the scan, etc.

Also, the robustness of the statistical model was demonstrated by the observation that the between-participant SD estimate was similar among all conditions.

Between-Trial Repeatability of Single- and 3-Image Measures

The between-trial repeatability was assessed independently for various measurement conditions (ie, sonographer-transducer combinations) by using the model described in Equation 1. For single-image measures, the data from the first image of the 3 images in an acquisition sequence were used when the 1-way random-effects model was applied. Therefore, there were 20 or 21 participants and 2 replicate measures (ie, 2 trials) per participant for each sonographer-transducer combination, regardless of whether single- or 3-image measures were assessed. The repeatability estimates were summarized in Table 3. For the single-image measures, the estimated ICC(1,1) for between-trial repeatability was greater than 0.7 for most conditions, and the ICC(1,2) was greater than 0.8 for most conditions. The ICCs estimated from 3-image measures were higher by up to 0.10 compared to those estimated from single-image measures.

The between-trial repeatability is a test-retest repeatability. This measure was a more clinically meaningful repeatability because the participants were repositioned (left the table and returned) between trials. The ICC values showed good between-trial repeatability if only a single image was acquired and analyzed to yield the AC and logBSC and excellent between-trial repeatability if 3 images were used to yield the AC and logBSC. It is not surprising that averaging the results from 3 images improved the between-trial repeatability. Similar to the between-image repeatability, the between-trial repeatability did not appear to be affected by the examined experimental conditions (including transducer and sonographer, but excluding the number of images used), as indicated by the similar ICC values between different transducers and sonographers.

Comparing Tables 2 and 3, the between-participant SD estimates were similar. The between-participant SD estimate in Table 2 was obtained by using the 1-way random-effects model, whereas the same estimate in Table 3 was obtained by using the 2-way random-effects model. The observation that the two models yielded similar between-participant SD estimates served as a corroboration of the data and algorithm.

The between-trial RC of single-image measures (Table 3) was approximately twice as large as the between-image RC (Table 2), suggesting better repeatability in the very short-term repeated condition without participant repositioning than in the test-retest condition with participant repositioning. Participant repositioning therefore appeared to adversely affect the repeatability, possibly because it was more difficult to scan the same region of the liver as the participant was repositioned. In other words, the liver might not be a perfectly homogeneous tissue in terms of AC and logBSC estimates.

The between-trial RC of 3-image measures was approximately 1.5 times as large as the between-image RC. The averaging appeared to have shortened the gap between the very short-term and the test-retest repeatabilities.

Between-Transducer Reproducibility of Single- and 3-Image Measures

The between-transducer reproducibility was assessed by using the 2-way random-effects model described in Equation 2. Participants and transducers were the 2 main random effects, and the trials were the replicates. For analysis based on single-image measures, only the data from the first image of the 3 images in an acquisition sequence were used. The 2-way random-effects

Table 3. Between-Trial Repeatability Estimates for Single- and 3-Image AC and BSC Measures Obtained Under Various Conditions, Calculated by Using the 2-Way Random-Effects Model

Conditions			Summary Statistics for AC, dB/cm-MHz					ICC Estimates for AC	
Participant Group	Transducer	No. of Images Averaged	Mean	Range	Between-Participant SD (95% CI)	Between-Trial Repeatability SD (95% CI)	RC (95% CI)	ICC(1,1) (95% CI)	ICC(1,2) (95% CI)
A	4C1	1	0.94	0.66, 1.18	0.12 (0.07, 0.19)	0.08 (0.06, 0.12)	0.23 (0.18, 0.34)	0.67 (0.34, 0.85)	0.80 (0.50, 0.92)
		3	0.94	0.67, 1.16	0.12 (0.08, 0.19)	0.06 (0.05, 0.09)	0.16 (0.13, 0.24)	0.81 (0.59, 0.92)	0.90 (0.74, 0.96)
A	6C1HD	1	0.97	0.73, 1.23	0.10 (0.06, 0.16)	0.07 (0.05, 0.09)	0.18 (0.14, 0.26)	0.71 (0.40, 0.87)	0.83 (0.57, 0.93)
		3	0.97	0.73, 1.21	0.11 (0.07, 0.16)	0.05 (0.04, 0.08)	0.15 (0.11, 0.21)	0.80 (0.56, 0.91)	0.89 (0.72, 0.95)
B	4C1	1	0.93	0.69, 1.25	0.12 (0.08, 0.18)	0.05 (0.04, 0.08)	0.15 (0.12, 0.22)	0.83 (0.63, 0.93)	0.91 (0.78, 0.96)
		3	0.93	0.69, 1.24	0.12 (0.08, 0.17)	0.05 (0.04, 0.07)	0.14 (0.11, 0.20)	0.84 (0.66, 0.93)	0.91 (0.79, 0.96)
B	6C1HD	1	0.93	0.56, 1.20	0.13 (0.09, 0.20)	0.08 (0.06, 0.11)	0.21 (0.17, 0.31)	0.74 (0.48, 0.89)	0.85 (0.64, 0.94)
		3	0.93	0.56, 1.21	0.13 (0.09, 0.20)	0.07 (0.05, 0.09)	0.18 (0.14, 0.26)	0.81 (0.59, 0.92)	0.89 (0.74, 0.96)
Conditions			**Summary Statistics for logBSC, dB**					**ICC Estimates for logBSC**	
Participant Group	Transducer	No. of Images Averaged	Mean	Range	Between-Participant SD (95% CI)	Between-Trial Repeatability SD (95% CI)	RC (95% CI)	ICC(1,1) (95% CI)	ICC(1,2) (95% CI)
A	4C1	1	–28.17	−39.23, −20.65	3.64 (1.87, 5.88)	3.12 (2.39, 4.51)	8.65 (6.62, 12.50)	0.58 (0.20, 0.81)	0.73 (0.33, 0.89)
		3	–28.17	−37.75, −20.76	3.85 (2.52, 5.90)	2.26 (1.73, 3.27)	6.27 (4.79, 9.05)	0.74 (0.46, 0.89)	0.85 (0.63, 0.94)
A	6C1HD	1	–26.55	−34.26, −14.63	3.49 (2.24, 5.39)	2.18 (1.67, 3.15)	6.04 (4.62, 8.72)	0.72 (0.42, 0.88)	0.84 (0.59, 0.93)
		3	–26.83	−34.40, −17.89	3.50 (2.37, 5.33)	1.85 (1.42, 2.67)	5.13 (3.92, 7.41)	0.78 (0.53, 0.91)	0.88 (0.70, 0.95)
B	4C1	1	–27.31	−38.54, −16.82	4.64 (3.25, 6.93)	2.23 (1.72, 3.19)	6.19 (4.76, 8.84)	0.81 (0.60, 0.92)	0.90 (0.75, 0.96)
		3	–27.35	−39.88, −17.51	4.47 (3.14, 6.66)	2.10 (1.61, 3.00)	5.81 (4.47, 8.31)	0.82 (0.61, 0.92)	0.90 (0.76, 0.96)
B	6C1HD	1	–25.46	−36.95, −15.91	4.41 (2.64, 6.85)	3.25 (2.50, 4.65)	9.01 (6.93, 12.87)	0.65 (0.32, 0.84)	0.79 (0.48, 0.91)
		3	–25.61	−37.20, −15.14	4.46 (2.80, 6.87)	3.03 (2.33, 4.32)	8.38 (6.45, 11.98)	0.69 (0.38, 0.86)	0.81 (0.55, 0.92)

Table 4. Transducer Reproducibility Estimates for Single- and 3-image AC and BSC Measures Obtained Under Various Conditions, Calculated by Using the 2-Way Random-Effects Model

Conditions		Summary Statistics for AC, dB/cm-MHz						
Participant Group	No. of Images Averaged	Mean	Range	Between-Participant SD (95% CI)	QIBA Reproducibility SD (95% CI)	Gauge Reproducibility SD	Between-Trial Repeatability SD (95% CI)	RDC (95% CI)
A	1	0.95	0.66, 1.23	0.11 (0.07, 0.16)	0.08 (0.07, 0.62)	0.03	0.08 (0.06, 0.10)	0.23 (0.20, 1.70)
	3	0.96	0.67, 1.21	0.10 (0.07, 0.16)	0.07 (0.06, 0.55)	0.05	0.06 (0.05, 0.07)	0.21 (0.17, 1.52)
B	1	0.93	0.56, 1.25	0.13 (0.09, 0.19)	0.07 (0.06, 0.08)	0	0.07 (0.06, 0.09)	0.18 (0.16, 0.23)
	3	0.93	0.56, 1.24	0.13 (0.09, 0.18)	0.06 (0.05, 0.09)	0	0.06 (0.05, 0.07)	0.16 (0.14, 0.26)
Conditions		**Summary Statistics for logBSC, dB**						
Participant Group	No. of Images Averaged	Mean	Range	Between-Participant SD (95% CI)	QIBA Reproducibility SD (95% CI)	Gauge Reproducibility SD	Between-Trial Repeatability SD (95% CI)	RDC (95% CI)
A	1	−27.36	−39.23, −14.63	3.56 (2.50, 5.39)	2.91 (2.51, 36.6)	1.09	2.69 (2.21, 3.45)	8.05 (6.94, 101)
	3	−27.50	−37.75, −17.89	3.46 (2.42, 5.26)	2.56 (2.18, 30.2)	1.51	2.07 (1.70, 2.64)	7.09 (6.04, 84.7)
B	1	−26.39	−38.54, −15.91	4.63 (3.45, 6.81)	2.90 (2.49, 41.9)	0.78	2.79 (2.30, 3.55)	8.02 (6.90, 116)
	3	−26.48	−39.88, −15.14	4.58 (3.42, 6.70)	2.68 (2.30, 39.4)	0.63	2.60 (2.15, 3.31)	7.42 (6.38, 109)

model yielded the between-transducer reproducibility estimates shown in Table 4. Additionally, between-trial repeatability without differentiating the transducers was also obtained as a result of the model.

The QIBA reproducibility SD estimates that included the transducer effects and the between-trial repeatability effects shown in Table 4 were close to the between-trial repeatability presented in Tables 3 and 4, and consequently, the RDC estimates in Table 4 were close to the RC estimates in Table 3. The closeness in the estimates between the QIBA reproducibility and the between-trial repeatability indicated that the transducers did not contribute significantly to the overall variability in the AC and logBSC measures. The variability caused by transducers alone was described by the Gauge reproducibility, and the estimated Gauge reproducibility SD values were lower than the between-trial repeatability SD values for all cases shown in Table 4. These results showed excellent between-transducer reproducibility: that is, the transducer did not contribute significantly to the measurement variability.

The between-participant SD and between-trial repeatability shown in Table 4 were close to those shown in Table 3, demonstrating consistency in the results obtained from different analyses. In Table 3, the between-participant SD and between-trial repeatability had to be estimated separately for the transducers, whereas in Table 4, the transducer effect became a model parameter.

Discussion

Quantitative US imaging is being increasingly investigated as an inexpensive, objective, and noninvasive method for diagnosing diseases and monitoring treatments using widely available clinical US systems. For QUS to gain wide acceptance, R&R must be demonstrated. Some of the key elements of R&R include very short-term repeatability (between image), on- and off-table repeatability (between trial), and reproducibility between different transducers, operators, manufacturers, measurement sites in the liver, etc. Although it is hard to quantify R&R across all the conditions in a single study, some elements believed important to the R&R of QUS measures in humans were examined.

Good to excellent overall R&R was demonstrated for AC and BSC measures obtained from 41 participants with known or suspected NAFLD. To better understand

the implications of the results, potential sources of variation in AC and BSC measures were examined. Technically, the AC and BSC were spatially averaged in the right liver lobe. Repeatability error has 2 sources: (A) intrinsic error of the measurement methods; and (B) biological variability. Error source A can be assessed by acquiring data from a spatially homogeneous liver-mimicking physical phantom. A previous phantom-based study[16] showed that the contribution of error source A was insignificant: the repeatability SDs were less than 0.02 dB/cm-MHz for the AC and 0.6 dB for the logBSC. In the human studies herein, both sources contributed to the repeatability error, which may explain why the between-image repeatability observed (repeatability SDs were between 0.03 and 0.05 dB/cm-MHz for the AC and between 1 and 2 dB for the logBSC) is somewhat worse than the phantom results. Error source B may result from liver heterogeneity or technical difficulty of scanning a human being. One way to address the effect of liver heterogeneity is to acquire multiple images and average together the measures. Hence, both single- measures and 3-image measures were assessed. Additional images may be used if better repeatability is desired, but the optimum number is yet to be determined. As a reference, 10 repeated measures are commonly used for liver stiffness assessment by acoustic radiation force impulse[21] and transient elastography.[15]

The between-image repeatability assesses the very short-term repeatability in a more controlled condition to help understand the sources of repeatability error. However, the between-image repeatability was less clinically demanding because the images shared the same acoustic window and target area of the liver with minimal transducer repositioning as well as sharing the same phantom scan, plus the participant was not repositioned. In comparison, the between-trial repeatability may be more relevant to clinical practice.

Good to excellent ICC values were observed for between-trial repeatability. The ICC(1,1) for the 3-image measures was greater than 0.8 for most cases, and the ICC(1,3) for the 3-image measures was in the range 0.85 to 0.9 for most cases. These ICC values demonstrate that the greatest portion of the overall variability originates from the between-participant variability rather than the between-trial variability when the measurements are acquired with the same transducer.

In addition to good repeatability, good transducer reproducibility was also observed, with the QIBA reproducibility SD only slightly greater than the between-trial repeatability SD. The error introduced by the transducer was lower than the repeatability error, as was also observed in the phantom study.[16] These AC and BSC measurement techniques were designed to remove system and operator dependencies by scanning a calibrated phantom, which explains the low variability introduced by transducers in both the phantom and in vivo human studies.

Quantitative ultrasound R&R measures are comparable with or better than other imaging modalities for liver assessment. For example, an overall ICC of 0.68 was reported for MR elastography used for assessing liver stiffness.[22] Acoustic radiation force impulse was shown to have an ICC between 0.7 and 0.9 for liver fibrosis assessment.[23] Another method for liver fibrosis assessment, transient elastography (FibroScan), has excellent overall inter-observer reproducibility with a reported ICC of up to 0.96.[24] However, the reproducibility of transient elastography depends on the liver fibrosis stage (ICC = 0.6 for fibrosis stage $\leq$1, and ICC = 0.99 for fibrosis stage $\geq$2).[25]

The focus of this R&R study was precision rather than accuracy. A thorough analysis of the accuracy is the topic of future studies. The accuracy is briefly discussed herein in 2 perspectives: (1) accuracy of measuring the AC and BSC by using the reference phantom technique; and (2) diagnostic accuracy of using the AC and BSC to quantify liver steatosis.

The reference phantom technique has been used in QUS research for more than 2 decades. It was originally proposed by Yao et al.[17] Portions of our previously published phantom data[16] are summarized as follows to demonstrate the accuracy of the reference phantom technique. The AC and BSC of 2 additional phantoms, P4 and P6 (CIRS, Inc), were measured with the reference phantom technique and compared with the independently calibrated AC and BSC values for P4 and P6. The AC and BSC were calibrated by using a broadband insertion loss method[26] and a planar reference method,[27] respectively. The independent calibration techniques have been validated by 2 interlaboratory measurement studies sponsored by the American Institute of Ultrasound in Medicine.[26,28] Two sonographers (A and B) each repeatedly scanned 3 phantoms (P2, P4, and P6) using 2 transducers (4C1 and 6C1HD) on the Siemens S3000 US scanner. A total of 60 data sets were acquired (A with 4C1, 11; A with 6C1HD, 10; B with

4C1, 20; and B with 6C1HD, 19). Each data set consisted of a set of scans of P2, P4, and P6 all under the same settings, whereas the settings varied across different data sets. Figure 5 shows box plots of the AC and BSC for P4 and P6 measured by the reference phantom technique with P2 as the reference. The box plots were grouped with sonographer and transducer on the same graph. Also presented in the box plots were 2 independent calibrations performed in September 2015 (designated cal1) and June 2016 (designated cal2), respectively. Each calibration represented the average of repeated calibrations performed by multiple operators. Excellent agreement was observed between the AC and BSC from the reference phantom technique and those from the 2 independent calibrations. Also, excellent agreement was observed between the 2 independent calibrations performed 9 months apart, implying stability of the phantom acoustic properties.

The diagnostic accuracy of using the AC and BSC to quantify hepatic steatosis can be found in 2 published studies[1,3] but is the focus of ongoing research. The results are briefly summarized as follows. The accuracy of the BSC in the diagnosis and quantification of hepatic steatosis was assessed in one of the previous studies[1] using the MRI-PDFF as a reference. The BSC was shown to be correlated with the MRI-PDFF (Spearman $\rho = 0.80$; $P < .0001$). The area under the curve value for using the BSC to detect NAFLD was 0.98 (95% confidence interval [CI], 0.95–1.00; $P < .0001$) in the training group. In the training and validation groups, the optimal BSC cutoff value detected NAFLD with 93% and 87% sensitivity, 97% and 91% specificity, 86% and 76% negative predictive values, and 99% and 95% positive predictive values, respectively. In the other study,[3] the diagnostic performance of the AC and BSC was assessed for predicting the histologically confirmed steatosis grade. The raw and cross-validated steatosis grading accuracies were 61.7% and 55.0%, respectively, for the AC, and 68.3% and 68.3% for the BSC. The accuracy of the AC and BSC for predicting the steatosis grade was shown to be higher than conventional US image interpretation (51.7% accuracy).

The accuracy of BSC measurement could be affected by subcutaneous fat. However, the subcutaneous fat did not appear to significantly affect the diagnostic accuracy of the BSC, as high diagnostic accuracy was demonstrated in the previous studies[1,3] without taking into account the effect of subcutaneous fat. Nevertheless, future studies should address the effect of subcutaneous fat to improve the BSC measurement accuracy, possibly by adopting an approach similar to that described in another study.[29] The subcutaneous fat does not affect the AC measurement as determined by the physical principles underlying the AC measurement algorithm; local attenuation, rather than attenuation above the liver, is being measured by the technique.

An important limitation of the described QUS technology is that it requires an external phantom and offline

Figure 5. Box plots of the AC (**A**) and logBSC (**B**) for P4 and P6 measured using the reference phantom technique with P2 as the reference and those independently calibrated in September 2015 and June 2016. Each calibration represented the average of repeated calibrations performed by multiple operators. The reference phantom technique results were grouped with sonographer and transducer on the same graph.

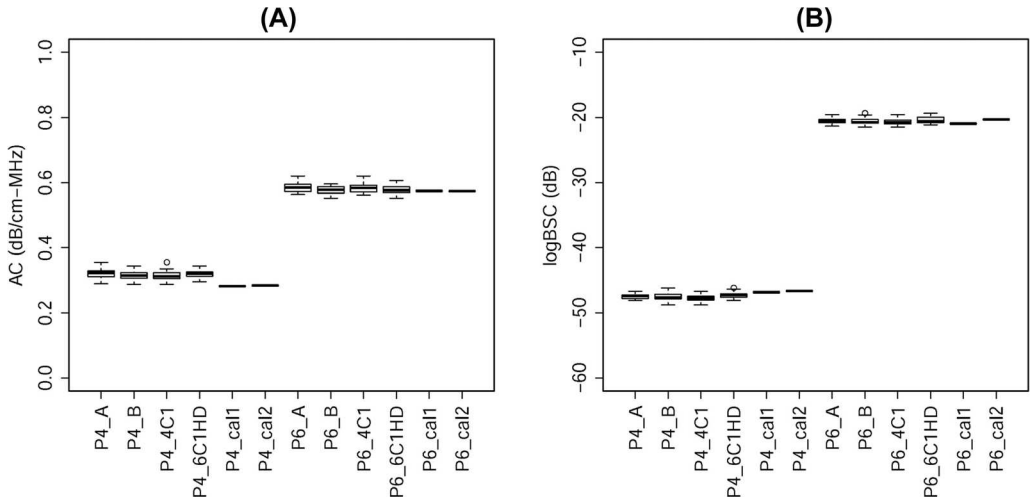

processing. Also, obtaining and working with RF data are challenging. Research is ongoing to streamline the work flow, with more manufacturers providing RF capabilities. We envision ultimate development of internally calibrated real-time QUS technology, which will facilitate its clinical translation. Another limitation of our study was the small sample size, which precluded analysis of some factors that may affect precision. We assessed some but not all components of variability, and future research is needed to assess other components, including scanner and sonographer reproducibility. This study was done at a single site, and external multiple-site validation of our results is needed.

In conclusion, hepatic AC and BSC measures using a reference phantom technique on a clinical scanner are repeatable and transducer reproducible in adults with known or suspected NAFLD. Further research is needed to evaluate additional factors that might affect the variability of the measurements.

References

1. Lin SC, Heba E, Wolfson T, et al. Noninvasive diagnosis of nonalcoholic fatty liver disease and quantification of liver fat using a new quantitative ultrasound technique. *Clin Gastroenterol Hepatol* 2014; 13: 1337–1345.e6.
2. Andre MP, Han A, Heba E, et al. Accurate diagnosis of nonalcoholic fatty liver disease in human participants via quantitative ultrasound. In: *Proceedings of the 2014 IEEE International Ultrasonics Symposium*. Piscataway, NJ: Institute of Electrical and Electronics Engineers; 2014:2375–2377.
3. Paige JS, Bernstein GS, Heba E, et al. A pilot comparative study of quantitative ultrasound, conventional ultrasonography, and magnetic resonance imaging for predicting histology-determined steatosis grade in adult nonalcoholic fatty liver disease. *AJR Am J Roentgenol* 2017; 208:W1–W10.
4. McFarlin BL, Balash J, Kumar V, et al. Development of an ultrasonic method to detect cervical remodeling in vivo in full-term pregnant women. *Ultrasound Med Biol* 2015; 41:2533–2539.
5. McFarlin BL, Kumar V, Bigelow TA, et al. Beyond cervical length: a pilot study of ultrasonic attenuation for early detection of preterm birth risk. *Ultrasound Med Biol* 2015; 41:3023–3029.
6. Sadeghi-Naini A, Papanicolau N, Falou O, et al. Quantitative ultrasound evaluation of tumor cell death response in locally advanced breast cancer patients receiving chemotherapy. *Clin Cancer Res* 2013; 19:2163–2173.
7. Sullivan DC, Obuchowski NA, Kessler LG, et al. Metrology standards for quantitative imaging biomarkers. *Radiology* 2015; 277:813–825.
8. Loomba R, Sanyal AJ. The global NAFLD epidemic. *Nat Rev Gastroenterol Hepatol* 2013; 10:686–690.
9. Dulai PS, Sirlin CB, Loomba R. MRI and MRE for non-invasive quantitative assessment of hepatic steatosis and fibrosis in NAFLD and NASH: clinical trials to clinical practice. *J Hepatol* 2016; 65:1006–1016.
10. Le TA, Chen J, Changchien C, et al. Effect of colesevelam on liver fat quantified by magnetic resonance in nonalcoholic steatohepatitis: a randomized controlled trial. *Hepatology* 2012; 56:922–932.
11. Loomba R, Sirlin CB, Ang B, et al. Ezetimibe for the treatment of nonalcoholic steatohepatitis: assessment by novel magnetic resonance imaging and magnetic resonance elastography in a randomized trial (MOZART trial). *Hepatology* 2015; 61:1239–1250.
12. Loomba R, Schork N, Chen CH, et al. Heritability of hepatic fibrosis and steatosis based on a prospective twin study. *Gastroenterology* 2015; 149:1784–1793.
13. Wong VW, Wong GL, Yeung DK, et al. Incidence of non-alcoholic fatty liver disease in Hong Kong: a population study with paired proton-magnetic resonance spectroscopy. *J Hepatol* 2015; 62:182–189.
14. Myers RP, Pollett A, Kirsch R, et al. Controlled attenuation parameter (CAP): a noninvasive method for the detection of hepatic steatosis based on transient elastography. *Liver Int* 2012; 32:902–910.
15. Chan WK, Mustapha N, Raihan N, Mahadeva S. Controlled attenuation parameter for the detection and quantification of hepatic steatosis in nonalcoholic fatty liver disease. *J Gastroenterol Hepatol* 2014; 29: 1470–1476.
16. Han A, Andre MP, Erdman JW, Loomba R, Sirlin CB, O'Brien WD Jr. Repeatability and reproducibility of a clinically based QUS phantom study and methodologies. *IEEE Trans Ultrason Ferroelectr Freq Control* 2017; 64:218–231.
17. Yao LX, Zagzebski JA, Madsen EL. Backscatter coefficient measurements using a reference phantom to extract depth-dependent instrumentation factors. *Ultrason Imaging* 1990; 12:58–70.
18. Burdick RK, Borror CM, Montgomery DC. *Design and Analysis of Gauge R&R Studies: Making Decisions With Confidence Intervals in Random and Mixed ANOVA Models*. Philadelphia, PA: Society for Industrial and Applied Mathematics; 2005.
19. Raunig DL, McShane LM, Pennello G, et al. Quantitative imaging biomarkers: a review of statistical methods for technical performance assessment. *Stat Methods Med Res* 2015; 24:27–67.
20. Shrout PE, Fleiss JL. Intraclass correlations: uses in assessing rater reliability. *Psychol Bull* 1979; 86:420–428.
21. Braticevici CF, Sporea I, Panaitescu E, Tribus L. Value of acoustic radiation force impulse imaging elastography for non-invasive evaluation of patients with nonalcoholic fatty liver disease. *Ultrasound Med Biol* 2013; 39:1942–1950.
22. Trout AT, Serai S, Mahley AD, et al. Liver stiffness measurements with MR elastography: agreement and repeatability across imaging systems, field strengths, and pulse sequences. *Radiology* 2016; 281:793–804.
23. Bota S, Sporea I, Sirli R, Popescu A, Danila M, Costachescu D. Intra- and interoperator reproducibility of acoustic radiation force impulse (ARFI) elastography: preliminary results. *Ultrasound Med Biol* 2012; 38:1103–1108.

24. Nobili V, Vizzutti F, Arena U, et al. Accuracy and reproducibility of transient elastography for the diagnosis of fibrosis in pediatric nonalcoholic steatohepatitis. *Hepatology* 2008; 48: 442–448.
25. Fraquelli M, Rigamonti C, Casazza G, et al. Reproducibility of transient elastography in the evaluation of liver fibrosis in patients with chronic liver disease. *Gut* 2007; 56:968–973.
26. Madsen EL, Dong F, Frank GR, et al. Interlaboratory comparison of ultrasonic backscatter, attenuation, and speed measurements. *J Ultrasound Med* 1999; 18:615–631.
27. Chen X, Phillips D, Schwarz KQ, Mottley JG, Parker KJ. The measurement of backscatter coefficient from a broadband pulse-echo system: a new formulation. *IEEE Trans Ultrason Ferroelectr Freq Control* 1997; 44:515–525.
28. Wear KA, Stiles TA, Frank GR, et al. Interlaboratory comparison of ultrasonic backscatter coefficient measurements from 2 to 9 MHz. *J Ultrasound Med* 2005; 24:1235–1250.
29. Wear KA, Garra BS, Hall TJ. Measurements of ultrasonic backscatter coefficients in human liver and kidney in vivo. *J Acoust Soc Am* 1995; 98:1852–1857.